Steel and Composite Structures, *Vol. 29, No. 2 (2018) 187-200*
DOI: https://doi.org/10.12989/scs.2018.29.2.187

Experimental and FE investigation of repairing deficient square CFST beams using FRP

Suzan A.A. Mustafa*

Department of Structural Engineering, Faculty of Engineering, Zagazig University, Egypt

(*Received March 5, 2018, Revised August 14, 2018, Accepted August 18, 2018*)

Abstract. This paper handles the repairing of deficient square Concrete-Filled Steel-Tube (CFST) beams subject to bending through an experimental and numerical program. Eight square-CFST beams were tested. A 5-mm artificial notch was induced at mid-span of seven beams, four of them were repaired by using CFRP sheets and two were repaired by using GFRP sheets. The beam deflection, strain and ultimate moments were recorded. It was found that providing different cut-off points for the different layers of FRP sheets prohibited failure at termination points due to stress concentrations. Using different lengths of FRP sheets around the notch retarded crack propagation and prevented FRP rupture at the crack position. Finite element analysis was then conducted and the proposed FE model was verified against the recorded experimental data. The influence of various parameters as FRP sheet length, tensile modulus and the number of layers were studied. The moment capacity of damaged square-CFST beams was improved up to 77.6% when repaired by using four layers of CFRP, however, this caused a dramatic decrease in beam deflection. U-wrapping of notched-CFST beam with 0.75 of its length provided a comparable behaviour as wrapping the full length of the beam.

Keywords: CFST; deficient; damaged; composite; FRP; beam; experimental; finite element

1. Introduction

Composite construction offers a remarkable balance between its advantages and its cost. Concrete filled steel tubular (CFST) sections are considered an innovative idea proved its efficiency in structural systems of tall buildings and bridges. Among these advantages; over a steel and reinforced concrete member; reduced cross section, higher stiffness and strength, high ductility and energy absorption, prevention of inward local buckling and finally, they serve as formwork during concrete infill. CFST sections powerfully carry compression and/or flexure. The flexural behavior of the CFST beams is acting much like hollow steel tubes. The concrete helps in moving the neutral-axis of the cross-section in the direction of the compression face of the beam.

Many factors cause deterioration of metallic structures, such as corrosion. In addition, some factors can hamper achieving the desired design strength as deficiencies at the design stage when using insufficient factor of safety or using low-grade materials. On the other hand, in many bridges, when the magnitude or intensity of the applied loads exceeds the design load capabilities, fatigue cracks are caused in the metallic members. This problem could be handled using two methods. The first method is demolition; complete or partial; then rebuild the section. The second method is retrofitting, which is considered more economic, less time duration and less service interruption. The traditional method to retrofit a steel structure has been the external bolting, riveting or welding of steel plates to the structural member, Seica and Packer (2007). Serious difficulties are faced when using these methods, for instance heavy lifting equipment to position the plates are needed, fitting in complex profiles is difficult and welding procedures is complicated. In addition, the added steel plates are likely to corrode and residual stresses are produced. In contrast, retrofitting using FRP materials do not reveal any of these drawbacks. Moreover, FRP composites are known with their environmental degradation resistance and have high modulus of elasticity and high strength/weight ratio Zhao and Zhang (2007).

Using FRP composites for strengthening steel members has started quite recently. Sen and Liby (1994) performed one of the first known researches on this topic by testing six composite beams under four-point bending. They used CFRP laminates for strengthening the tension flange of the steel beam. Although they recorded significant enhancement in the ultimate strength, elastic response of the beams needed to be improved. In 2005, Yang *et al*. (2005) investigated the bond behavior of CFRP to steel members and they recommended a suitable adhesive for this purpose. Photiou *et al*. (2006) used two different wrapping configurations of ultra-high modulus and high-modulus CFRP for strengthening artificially degraded steel beams with rectangular cross section under four-point loading. The beams strengthened by high-modulus CFRP exhibited more ductile response compared to those strengthened with ultra-high-modulus CFRP. Teng and Hu (2007) studied the effect of FRP confining hollow steel tubes experimentally and numerically. They found that this technique is very

*Corresponding author, Associate Professor,
E-mail: suzanaa1@zu.edu.eg

http://www.techno-press.org/?journal=scs&subpage=6
ISSN: 1229-9367 (Print), 1598-6233 (Online)

promising for retrofitting. Fawzia *et al*. (2007) studied strengthening very high strength circular steel tubes subject to tension, by using CFRP. They showed the superiority of high modulus CFRP in retrofitting steel tubes and concluded that the effective bond length was around 50 mm and 75 mm for bonding normal modulus and high modulus CFRP to the steel tube, respectively. Zhong *et al*. (2007) investigated strengthening fire-damaged circular and square concrete filled steel tube specimens under axial compression and bending using uni-directional CFRP sheets. An increase in the longitudinal stiffness and the load carrying capacity of CFRP-rehabilitated CFST members was reported with the increasing number of CFRP layers. Meanwhile the ductility of the specimens was decreased. In another research, Zhong and Han (2007) studied rehabilitation of fire-exposed CFST beam columns using CFRP composites. The results assured the enhancement of the load carrying capacity of the section when using CFRP sheets; however the effect on stiffness was not obvious.

A number of researches handled the rehabilitation or strengthening of steel I-beams using FRP composites, for example Tavakkolizadeh and Saadatmanesh (2003), Kim and Harries (2011), Colombi and Fava (2015), and Yousefi *et al*. (2017). A limited number of studies considered the rehabilitation of hollow steel tubular beams using the FRP material, among them Elchalakani presented two researches in (2014a, b), Chen *et al*. (2015) and Mahdi *et al*. (2018). To date, only Al Zand *et al*. (2017) studied the rehabilitation of damaged rectangular CFST beams using CFRP sheets under three point bending. They examined one damaged rectangular CFST beam without repair in addition to a repaired CFST beam using two layers of CFRP sheet covering the beam full length. They concluded that applying the CFRP sheet to the damaged beam improved its capacity by approximately 63% and improved its ductility index by approximately 60-65%, which was still lower than the ductility value of the undamaged un-strengthened beam.

Due to the scarcity of researches concerning retrofitting of deficient CFST beams using FRP composites, an investigation on retrofitting deficient square CFST beams is presented in this research. An experimental study on eight square CFST beams was carried out. An artificial cutting (notch) at mid-span of seven beams was created. Four CFST deficient beams were repaired by using uni-directional CFRP sheets, while two more beams were repaired by using uni-directional GFRP sheets. Different schemes of FRP sheets were adopted to examine its efficiency in retrofitting the notched CFST square beams. Moreover, a three dimensional finite element model was presented and validated using the experimental data. The FE model simulated the repaired, unrepaired, damaged and undamaged beams. The effect of some parameters was studied as the number of FRP layers, FRP sheet length and the FRP tensile modulus.

2. Experimental investigation

2.1 Details of tested specimen

Eight square hollow steel tubes with 100 mm side length and thickness of 2.3 mm were tested. For all CFST beams, the overall length was 1500 mm, while the clear span between supports was 1300 mm. The eight beams were filled with concrete and a 5 mm wide crack was induced at mid span of seven beams. Two beams were used as control beams without any repair. The first control beam was designated as RU refers to the control beam without crack, while the second control beam was designated as RD refers to the control beam with crack. Four beams were repaired using uni-directional CFRP sheets in addition to two beams were repaired by using unidirectional GFRP sheets. All of the FRP sheets were used with U-shape (covering the lower flange and the two webs of the CFST). Different lengths of the FRP sheets were adopted forming different repairing schemes. All the used repairing schemes had the same FRP total area for the sake of comparison. The used schemes are illustrated in Table 1. The dimensions of the tested beams and the number of layers of FRP strips are summarized in Table 2.

2.2 Specimen preparation

Before filling the tubes with concrete, the inner surface of the tubes was cleaned and the lower ends of the square tubes were covered by plastic sheets to prevent leakage. The tubes were fixed in a vertical position, and then the concrete was poured from the upper side in five layers. Each layer was compacted using a steel rod. The concrete was cured for 28 days before testing. A crack was induced by a 5 mm cut at the middle of the lower flange of the steel tubes of seven beams, as shown in Fig. 1. To insure a good bond between the steel tubes and the FRP sheets, tiny hair scratches were induced at the outer surfaces of the steel tubes; along and across the beam; using low speed electric grinder. All surfaces were cleaned several times with acetone before adhesive and FRP application. The adhesive used to bond the FRP sheets to the steel tubes was a mix of two components; resin and hardener; were perfectly mixed with a ratio of 4:1 by weight, as directed by the manufacturer precautions. The adhesive was applied then the FRP sheets were placed at the specified positions immediately so that the FRP sheet is immersed totally in the epoxy. A roller was used to insure uniform thickness of the adhesive and to remove air voids, as shown in Fig. 1. In specimens with several layers of FRP sheets, the process was repeated. The repaired CFST beams are cured at room temperature for ten days before testing. A strain gauge was attached at the middle of the lower face of each beam. Course sand paper and soft sand paper were used to prepare the positions at which the strain gauges were glued.

2.3 Material properties

Steel tubes with 100 mm × 100 mm square cross-section and 2.3 mm thickness were used. According to the ASTM-E8/E8M, three coupons were cut and prepared to determine the mechanical properties of the steel tubes. The tests reviled on average yield strength of 440.3 Mpa and ultimate strength of 479 Mpa. The concrete mix was designed to achieve a compressive strength of 25 Mpa. Three concrete cubes were prepared during concrete casting

Table 1 Beam cross section and repairing schemes

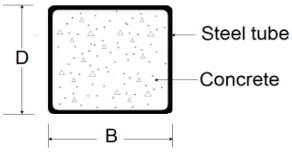 Reference beams RU & RD	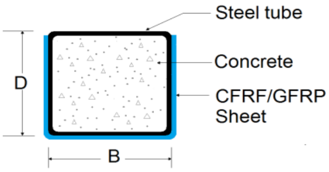 Repaired beams
Beams repaired using CFRP sheets	
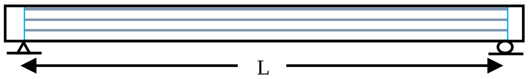	Beam D1 Two layers of CFRP sheet parallel to the beam with length = L
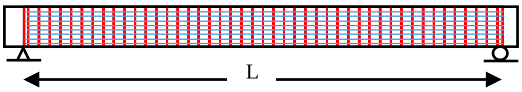	Beam D2 1st layer of CFRP sheet parallel to the beam with length = L 2nd layer of CFRP sheet transverse to the beam with length = L
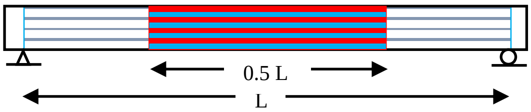	Beam D3 1st layer of CFRP sheet parallel to the beam with length = L 2nd and 3rd layers of CFRP sheet parallel to the beam, each with length = 0.5 L
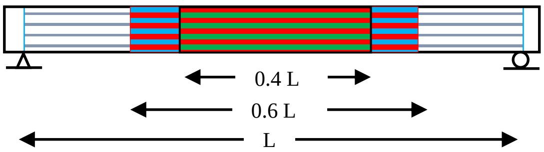	Beams D4 1st layer of CFRP sheet parallel to the beam with length = L 2nd layer of CFRP Sheet parallel to the beam with length = 0.6 L 3rd layer of CFRP Sheet parallel to the beam with length = 0.4 L
Beams repaired using GFRP sheets	
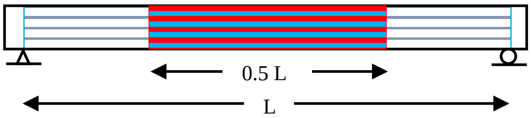	Beam D5 1st layer of GFRP Sheet parallel to the beam with length = L 2nd and 3rd layers of GFRP Sheet parallel to the beam, each with length = 0.5 L
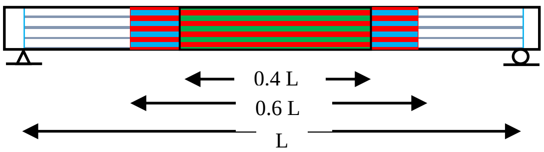	Beam D6 1st layer of GFRP Sheet parallel to the beam with length = L 2nd layer of GFRP Sheet parallel to the beam with length = 0.6 L 3rd layer of GFRP Sheet parallel to the beam with length = 0.4 L

for compressive strength test. The cubes and the specimens were cured in laboratory and tested after 28 days. The average concrete strength obtained was 28.7 Mpa.

Two different types of FRP were used for repairing the deficient beams; Sikawrap-230C (unidirectional carbon fibre fabric) (CFRP) and Sikawrap-430G (unidirectional glass fibre fabric) (GFRP). A two-component adhesive; Sikadur-330 Normal epoxy; was used for bonding the FRP sheets to the steel beams and to each other. The adhesive was considered as a thin layer of about 1.00 mm between FRP sheets and the steel tubes. The properties of FRP types and the adhesive provided by the manufacturer are detailed in Table 3.

2.4 Schematic of the FRP sheets

Six CFST beams repaired with FRP sheets were tested. The FRP sheets were applied in a U-shape surrounding the lower flange and the two webs of the steel tubes; as shown in Table 1. Each beam was repaired using two pieces of the FRP sheet with a total length equals the whole clear span 1300 mm. The first beam, D1, was repaired with the two layers of the CFRP sheet parallel to the beam extending over the whole clear span. The second beam, D2, was repaired with two layers of CFRP sheet one of them was parallel to the beam and the other layer with the fibers transverse to the beam. For the third beam D3, the first CFRP piece was applied with the fibers parallel to the beam. The second piece was divided into two equal parts each of which with length equals 50% of the clear span (0.5 L), and they were centered on the beam, as illustrated in Table 1. The fourth beam, D4, was repaired with the first piece parallel to the beam. The second CFRP piece was divided into two parts with lengths equal 0.60 L and 0.40 L of the clear span length. All the repairing parts were centered on beam D4. Beams D5 and D6 were repaired with the same patterns of D3 and D4, respectively using GFRP sheets instead of CFRP sheet. Details and arrangements for all repaired beams are illustrated in Table 1.

Table 2 Repairing schemes of tested CFST specimens

Beam designation	FRP type	FRP layers	FRP fiber direction	FRP Length ratio %
RU	-	-	-	-
RD	-	-	-	-
D1	CFRP	Layer1	P	100
		Layer 2	P	100
D2	CFRP	Layer 1	P	100
		Layer 2	T	100
D3	CFRP	Layer 1	P	100
		Layer 2	P	50
		Layer 3	P	50
D4	CFRP	Layer 1	P	100
		Layer 2	P	60
		Layer 3	P	40
D5	GFRP	Layer 1	P	100
		Layer 2	P	50
		Layer 3	P	50
D6	GFRP	Layer 1	P	100
		Layer 2	P	60
		Layer 3	P	40

* For all beams:
Steel tube dimensions (B×D×t) = 100×100×2.3 mm
Total length of FRP sheets = 260 mm

Table 3 Material properties of FRP and Epoxy

Material	Thickness (mm) *	*E* (Gpa)	Ultimate tensile strength (Mpa)	Ultimate strain %
CFRP	0.128	234	4300	1.8
GFRP	0.172	76	3400	2.8
Epoxy	-	4.5	30	0.9

* Sheet thickness was considered as the nominal thickness of the dry fiber

Table 4 Summary of experimental results

Beam	Mu (kN.m)	Δ_y* (mm)	Δ_u**	μ_d***	$\frac{M_u}{M_{u(RU)}}$	$\frac{M_u}{M_{u(RD)}}$	Failure mode
RU	22.30	5.60	30.5	5.44	1.000	1.524	A
RD	14.63	3.20	9.8	3.06	0.656	1.000	A&B
D1	22.12	3.30	12.1	3.67	0.992	1.512	A&C
D2	18.86	3.40	13.2	3.88	0.846	1.289	A&D
D3	22.56	4.80	19.5	4.06	1.012	1.542	A&B&C
D4	24.10	3.60	14.2	3.94	1.081	1.647	A&B&C
D5	19.44	5.50	23.3	4.23	0.872	1.329	A&B&C
D6	20.8	4.80	19.6	4.08	0.933	1.422	A&B&C

*Δ_y: Deflection at yield,
**Δ_u: Deflection at ultimate load,
***μ_d: Displacement ductility (ratio of deflection at the ultimate load to deflection at yielding),
A: Local buckling at top flange, B: Crack propagation,
C: FRP debonding, D: FRP rupture

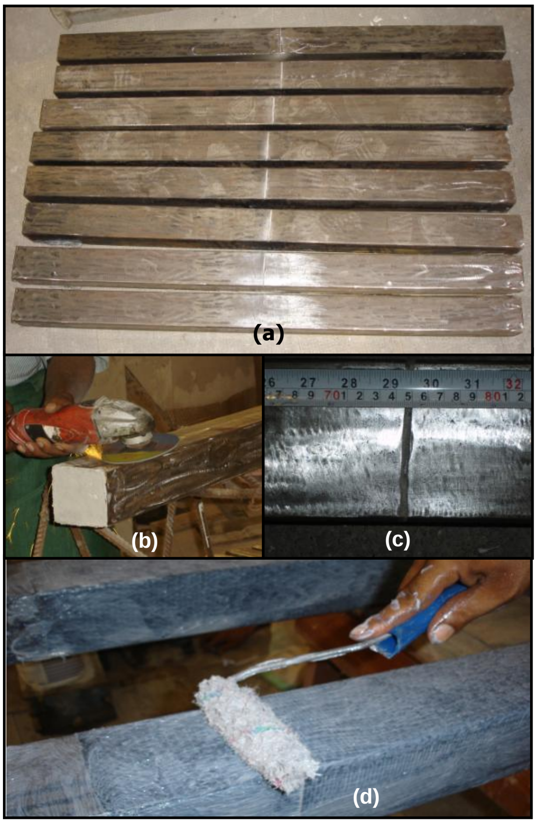

Fig. 1 CFST beams: (a) Beams; (b) Steel tube grinding; (c) 5-mm artificial cut; (d) FRP application

2.5 Test setup and instrumentation

Experiments were performed using a 250 kN capacity hydraulic jack applying four-point loading system with a loading rate between 3-5 kN/min. The experimental setup is shown in Fig. 2. The readings of beam deflection at mid-span and at the quarter of the beams were recorded by using

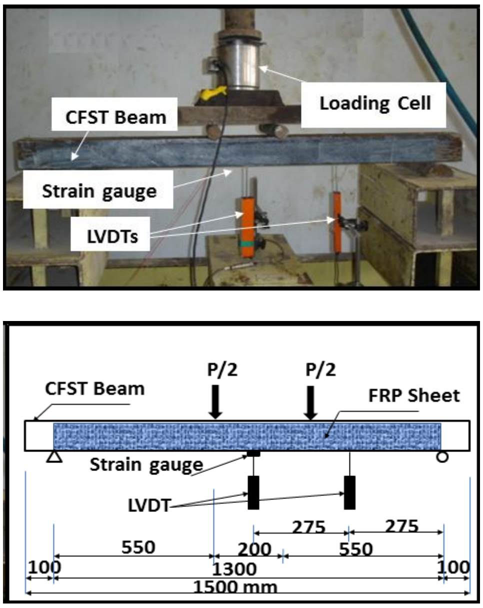

Fig. 2 Loading arrangement and test details

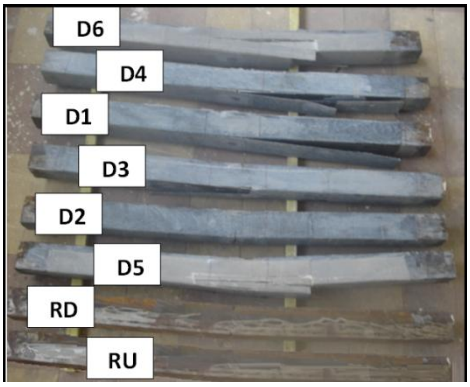

Fig. 3 Tested specimens

two Linear Variable Displacement Transducers (LVDT). Strain measurements were recorded using strain gauges directly glued at the center of the bottom side of each beam. A Data Logger was used for collecting the load value, deflection and strains from the testing machine, LVDTs and strain gauges, respectively.

3. Experimental results and discussion

Table 4 summarizes the basic experimental findings of the tested beams in this study. The ultimate moment (M_u), deflection at yield Δ_y) and deflection at ultimate load Δ_u), displacement ductility factor μ_d, and mode of failure of each specimen are included in the table. All beams reached their ultimate moments with no change in the beams' cross sections and no unexpected lateral movement that could have affected the results was noticed. Furthermore, no slippage between the concrete core and the steel tube at the ends of the tested specimens was observed.

3.1 Failure modes

Fig. 3 shows the failure of the tested specimens. For all beams, local buckling at the top flange was observed in the vicinity of the loading points starting from a load value close to the ultimate load. This was noticed for repaired and unrepaired beams; as shown in Fig. 4(a), for specimen RU as an example for unrepaired beam and D1 as an example for repaired beam. The unrepaired composite beam (RD) failed due to fracture in the steel tube in addition to the local buckling at the top flange. Fig. 4(b) shows the beginning of crack propagation of the steel tube.

3.1.1 CFST beams repaired by CFRP

For D1 which was wrapped by two layers of CFRP parallel to the beam, longitudinal rupture of CFRP layers initiated from the edge of the CFRP sheet in addition to local buckling at the middle of top flange of the steel tube, as shown in Fig. 4(c). Beam D2 was repaired by two layers of CFRP sheet. One layer was parallel to the beam and the other layer was transverse to the beam. Small CFRP sheet cracking was noticed at the position of the artificial crack at load of about 92% of the beam ultimate load; as illustrated in Fig. 4(d). Then gradual rupture of the CFRP sheet occurred accompanied by propagation of the artificial crack in addition to local buckling at the middle of top flange of steel tube. No CFRP debonding failure or sudden longitudinal rupture failure was observed in this beam. This may be attributed to the existence of the second layer of CFRP sheet with the fibers perpendicular to the beam.

Beams D3 and D4 were strengthen using two strips of the CFRP sheet each of which had the full length of the tested span, 1300 mm. The first layer in each beam was applied parallel to the beam. The second layer in Beam D3 was divided equally into two pieces and applied at the center of the beam. While the second layer in Beam D4 was divided into two pieces with lengths of 0.40 L and 0.60 L of the tested span length; as detailed in Table 1. Longitudinal rupture of the CFRP sheets was observed in beam D3 in the second and third layers with lengths of 0.50 L of the beam span, as illustrated in Fig. 4(e). This rupture went along with explosive sound, then, debonding of CFRP at mid-span at the top of the webs. Local buckling was perceived at the middle of the top flange of the steel tube accompanied by crack propagation through the steel tube webs. In beam D4, longitudinal rupture in the CFRP sheets at about 94% of the ultimate load, and then local buckling at mid-span in the top flange of the steel tube started. Debonding in the second layer (with length 0.40 L of the beam span) of the CFRP sheet began then debonding at the far edge of the first layer of CFRP sheet toke place. This was accompanied by crack propagation through the steel beam webs and an increase in the top flange local buckling. The failure of beam D4 is illustrated in Fig. 4(f).

3.1.2 CFST beams repaired by GFRP

CFST beams D5 and D6 were repaired the same way of beams D3 and D4, respectively but with GFRP sheet. In beam D5, debonding of the GFRP sheet was observed at layers with length equals 0.50 L of the clear span and local buckling at the top flange at the middle of the beam was noticed. In addition, crack propagation started and the steel tube was fractured, as shown in Fig. 5(a). In beam D6, longitudinal fracture in the GFRP started along the edges of the CFST beam accompanied by local buckling in the top flange of the steel tube. The crack began propagation and slippage between the GFRP and the steel tube webs occurred, as shown in Fig. 5(b).

Since the peeling stress is directly proportional to the bending stress, debonding failure occurred in all specimens with two layers of length 0.50 L of the beam span due to the huge peeling stress that produce at mid-span at which the bending stress is maximum. The same conclusion was observed in Sundarraja and Prabhu (2013), Al Zand *et al*. (2015) and (2016). When the two layers of the FRP sheet were equal, it helped peeling of the FRP sheets. Using different lengths of FRP sheets helped in preventing peeling of all the additional layers at the same time and delayed the beam failure. Using the additional layers of the FRP sheets over the beam notch retarded crack propagation and prevented rupture of the sheet at the notch position.

3.2 Effect of FRP retrofitting on CFST beams

Fig. 6(a) presents the moment versus mid-span

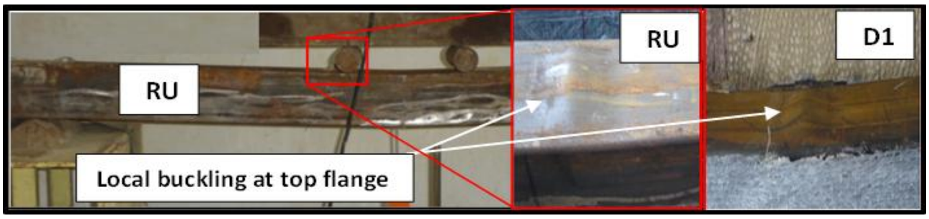

(a)

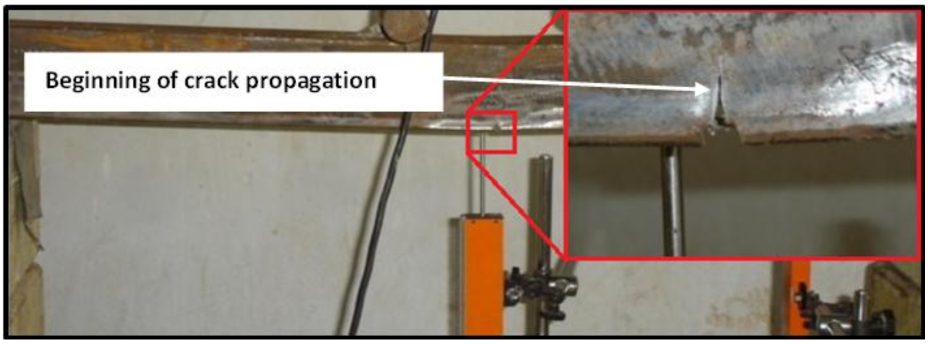

(b)

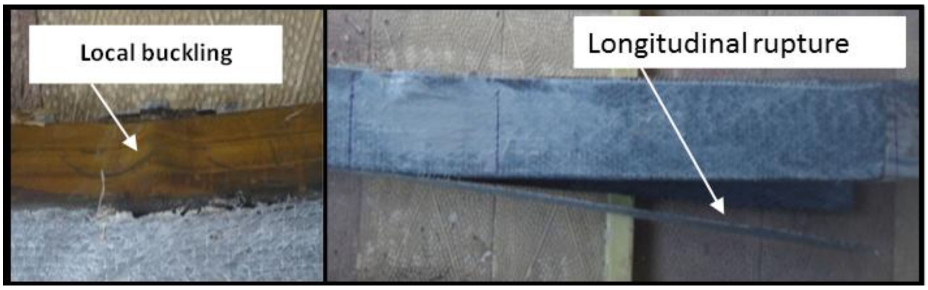

(c)

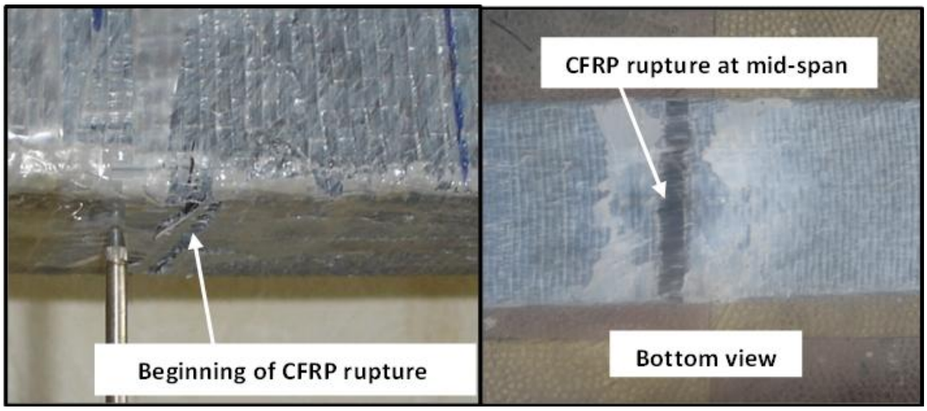

(d)

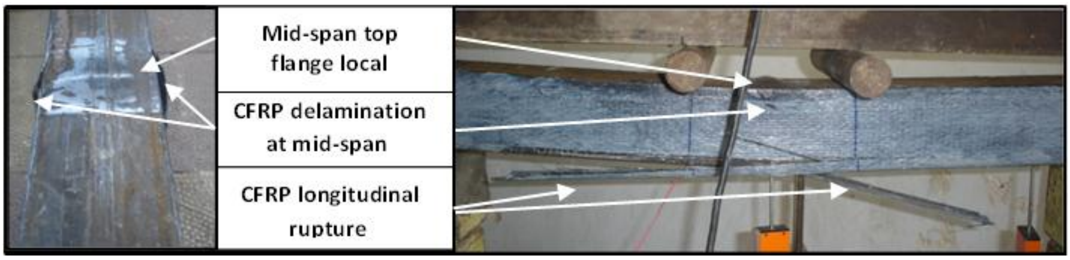

(e)

Fig. 4 Failure of tested specimens with CFRP: (a) Local buckling at top flange, (b) Beginning of crack propagation in specimen RD (c) Failure of beam D1, (d) Failure of beam D2, (e) failure of beam D3,

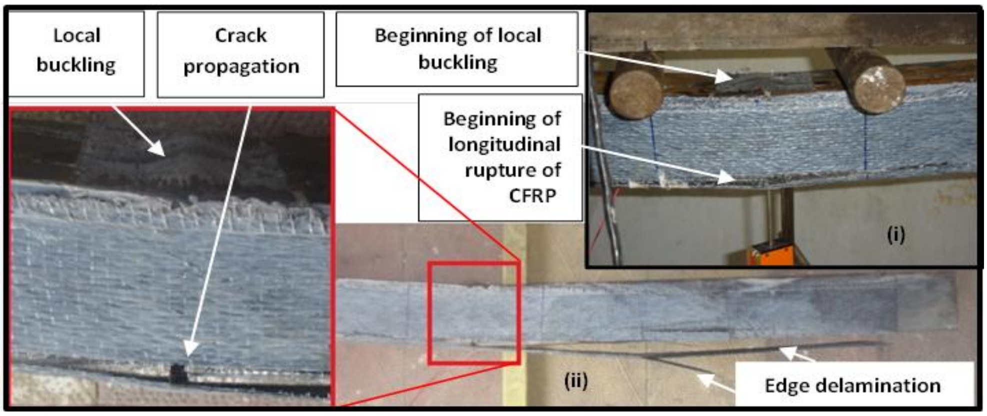

(f)

Fig. 4 Continued

deflection of the deficient beams repaired with CFRP sheets and the two reference beams (with and without notch). All beams showed elastic behavior at the beginning of loading. Then, inelastic response was observed until the ultimate load was reached. In un-deficient reference beam (RU), the ultimate moment capacity was about 22.30 kN.m. Noticeable increase in the beam deflection was observed with nearly the same value of the moment until the beam failed at a deflection equal 30.50 mm. Providing an artificial notch at the bottom flange of the steel tube reduced the moment capacity of the CFST beam by about 34.4%, as illustrated in Table 4 for the deficient reference beam (RD). When the beam reached its ultimate moment capacity, which was about 14.63 kN.m, the load decreased rapidly with steel beam fracture. Wrapping the full length of the deficient CFST beam with two layers of CFRP sheets parallel to the beam (beam D1) increased the ultimate moment capacity of the beam by about 51%. The moment capacity of this beam reached 22.12 kN.m which aproximatly restored 99.2% of the reference un-deficient beam. The application of the two full length CFRP sheet with one layer parallel to the beam and the other was transverse to the beam (beam D2) improved the moment capacity of the deficient beam of about 28.9%, as detailed in Table 4. This repairing pattern lead to a lower enhancement in the beam load capacity than using two parallel layers and consequently could not restore the full capacity of the reference beam (RU), however it prevented the longitudinal CFRP rapture and showed a gradual failure, as shown in Fig. 6(a).

Adopting the two suggested wrapping techniques in D3 and D4; one CFRP layer covers the whole span of the beam and the second CFRP layer into two equal pieces (in D3) and two unequal pieces (in D4) increased the beam ultimate capacity by 54.2% and 64.7%, respectively. The moment capacity of the un-deficient reference beam was exceeded by 1.2% and 8.1% in D3 and D4, respectively. However, using these wrapping schemes with GFRP sheets in beams D5 and D6 increased the deficient CFST beam capacity by 32.9% and 42.2%, respectively. These were 22% lower than the enhancement provided by the CFRP sheet in D3 and D4. This is due to the low elastic modulus of the GFRP compared with the CFRP.

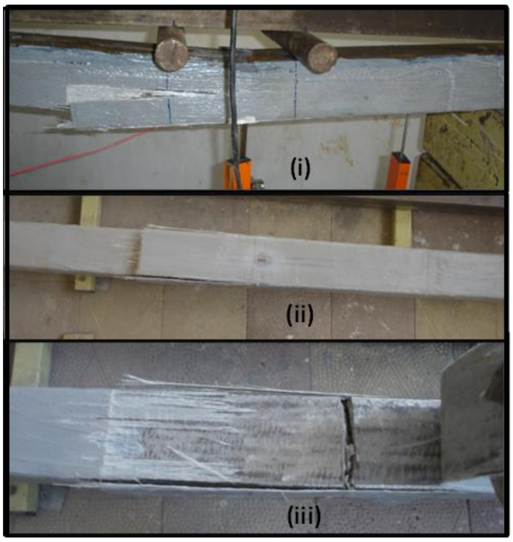

(a)

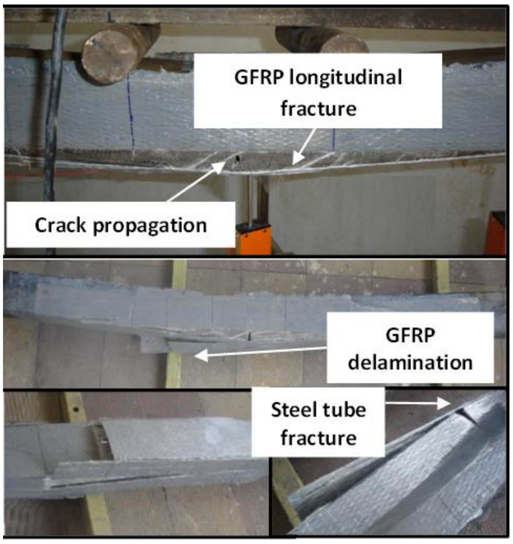

(b)

Fig. 5 Failure of tested specimens with GFRP: (a) Failure of beam D5: (i) Rupture and debonding of GFRP at langth 0.5 L; (ii) Bottom view; (iii) Fracture of CFST beam; (b)failure of beam D6

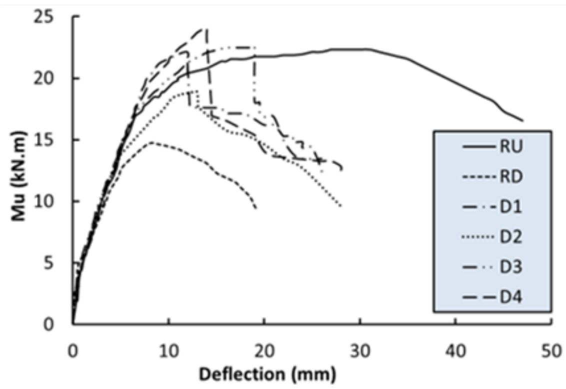

(a) Specimens repaired by using CFRP sheets

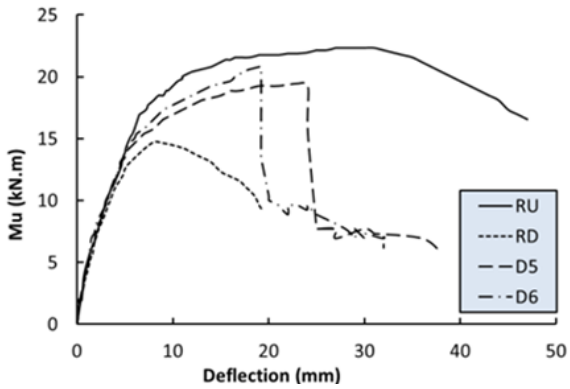

(b) Specimens repaired by using GFRP sheets

Fig. 6 Moment-deflection curves

3.3 Ductility index and beam strains

Ductility is an essential property for a structural element because it delivers warning of approaching failure. In terms of displacements, ductility is calculated by dividing the ultimate deflection by the deflection during the first yield, as detailed in Table 4. This index could easily indicate the capability of the CFST beam to withstand inelastic deformation before failure. The ductility index of the un-deficient reference specimen (RU) was 5.44. When the beam was notched (beam RD), its ductility index decreased significantly to 3.06. The ductility of the notched beams was increased when they were wrapped by CFRP sheets and GFRP sheets, as shown in Fig. 7. Although some of these wrapping techniques could restore the original moment capacity of the un-deficient reference beam, but none of them managed to bring back its ductility. The maximum increase in the notched beam ductility was achieved when using the GFRP by 38% and 33% in D5 and D6 respectively. Using the same wrapping techniques by CFRP sheet increased the CFST beam ductility by 32.7% and 28.8% in beams D3 and D4, respectively. Covering the full tested length of the CFST beam with two layers of the CFRP parallel to the beam (beam D1) increased the notched beam ductility by about 20%. Whereas if one of the sheets was glued parallel to the beam and the other was glued transverse to the beam, the notched beam ductility increased by 26.8%, as in beam D2. As illustrated in Fig. 7, the ductility behavior of all repaired notched CFST beams did not exceed 77.8% of that of the un-notched reference beam (RU). This may be attributed to the low strain limit of the FRP sheets compared to steel. The moment versus strains in the tension sides of the CFST beams at mid-span of the un-deficient reference beams and the repaired beams are shown in Fig. 8. In the reference beam (RU), the turning point in the curve indicated the yielding in the lower surface of the steel tube after the elastic response of the beam under the load. While in the repaired CFST beams, the strain readings increased until failure in the FRP laminates occurred. In beams D2 and D5, when the moment reached about 12 kN.m, constant strain gauge readings were observed with the increase of loading. Similar behavior was recorded by Sallam (2010). Unreliable load-strain behavior was observed after the lower flange of the steel tube started yielding. The strain remained constant with the increase in loading then instability occurred up to failure. Other explanations were provided in Sallam (2010) stating that after yielding any discrepancy in strain may be due to the short gauge length of the strain gauges used or the exact location of the plastic hinge within the constant moment region relative to the gauge position.

4. Finite element analysis

A nonlinear three-dimensional finite-element model was prepared by ANSYS V.15 program to investigate the structural behavior of repaired and unrepaired square CFST beams. All tested beams were simulated and the results were compared to validate the proposed model. Due to symmetry, only one quarter of the beam was modeled. Fig. 9 shows a typical shape of the simulated beams. The symmetric planes of the beam, loading and support positions are illustrated in the figure. The nodes corresponding to the support positions were restrained according to support conditions. Beam symmetry was appropriately modeled by restraining the nodes corresponding to the plane of symmetry by suitable boundary conditions. Using load steps and sub-steps, the load was applied gradually to the beam with loading increments similar to the loading pattern used in the experimental tests. Convergence study was adopted to obtain adequate accuracy of repaired CFST beam results concerning deformations and stresses. This was achieved with 10728 elements and 11463 nodes for quarter beam. The Elements' description, material properties and validation of the FE model, are discussed herein:

4.1 Elements' description

Five different elements were used to designate the model of the repaired CFST beam parts. The first element was eight-node SOLSH190 element. It was used for simulating steel tubes since it is capable of representing a wide range of thickness; from thin to moderately thick element. Each node has three translational DOF. It has plasticity, stress stiffening, large deflection, and large strain capabilities. The second element represented the concrete core; SOLID65; which has eight nodes with three degrees of freedom at each node; translations in the nodal *x*, *y*, and *z* directions. The element is capable of cracking in tension in three orthogonal directions and crushing in compression during the load steps. The third element was SHELL181, and used to represent the FRP sheets. It is layered element suitable for modeling composite shells. It has four nodes with six DOF at each node. The orientation and the orthotropic material properties were specified for each layer. The FRP sheets were attached to the steel surface using three-dimensional surface-to-surface contact pair elements (CONTA174 and TARGE170). CONTA174 was adopted to implement the contact and sliding between surfaces. The element takes the geometric features of the element face of which it is attached to. TARGE170 was adopted to implement 3-D target surface for the related contact elements. The steel elements were chosen as target-surfaces and the FRP elements were chosen as contact surfaces in the repaired parts of the CFST beams.

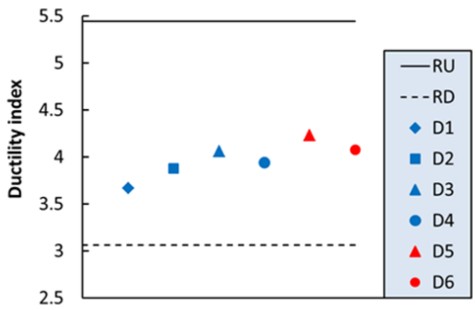

Fig. 7 Ductility index of tested beams

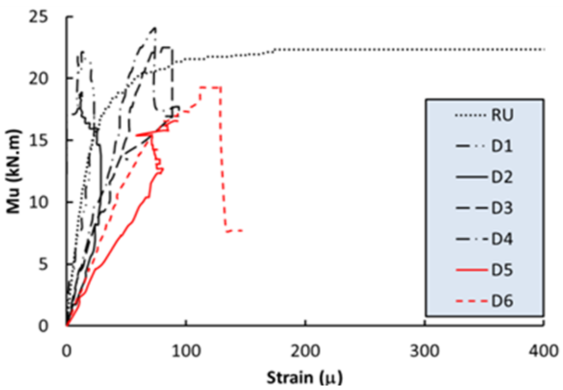

Fig. 8 Strain in tested beams

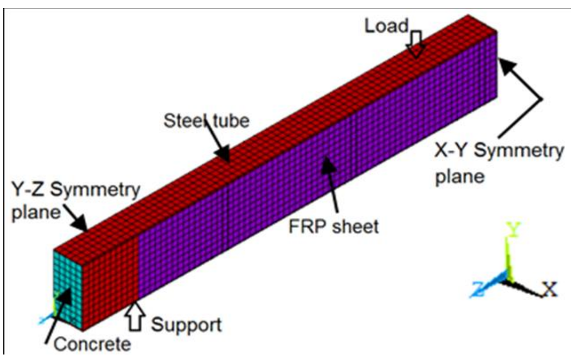

Fig. 9 Typical shape of finite element model

4.2 Material properties

A bi-linear stress-strain relationship was adopted for modeling the steel tube material; as shown in Fig. 10(a). Yield and ultimate stress values were considered from testing the coupons as detailed in Table 3. Steel material properties were assumed to be identical in tension and compression. The stress-strain relationship for concrete is shown in Fig. 10(b), and it can be divided into two stages. The first stage, from zero to the first point on the curve; about 30% of the maximum compressive strength; the relation is linearly elastic and the strain is calculated according to Eq. (1), where (f) is the concrete stress at any strain value (ε) and (Ec) is the modulus of elasticity of concrete. In the second stage, a gradual increase in the stress is considered up to the maximum compressive strength forming the following points which were calculated from Eq. (2); (Gere 1997). Strain at the ultimate compressive strength ($\varepsilon 0$) can be obtained from Eq. (3), which indicates occurrence of crushing failure. The value of the uni-axial crushing stress was considered as found in the experimental tests; Table 3, while the uni-axial cracking stress was taken about 10% of the compressive strength. The tensile crack factor was considered 0.5 to avoid divergent problems at the first crack point, and to avoid the encountered other convergence problems, the shear transfer coefficient was taken 0.3 for open crack and 0.8 for closed crack. The CFRP and GFRP sheets were modeled as orthotropic materials. Number of layers, thickness of each layer, orientation of the fibers in each layer, elastic moduli in the three directions, shear moduli in the three directions and poisson's ratios were specified for each FRP composite

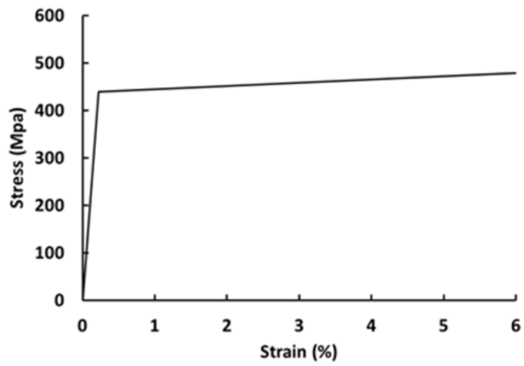

(a) Steel

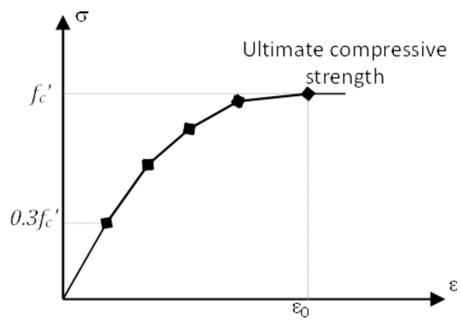

(b) Concrete

Fig. 10 Stress-strain relationships

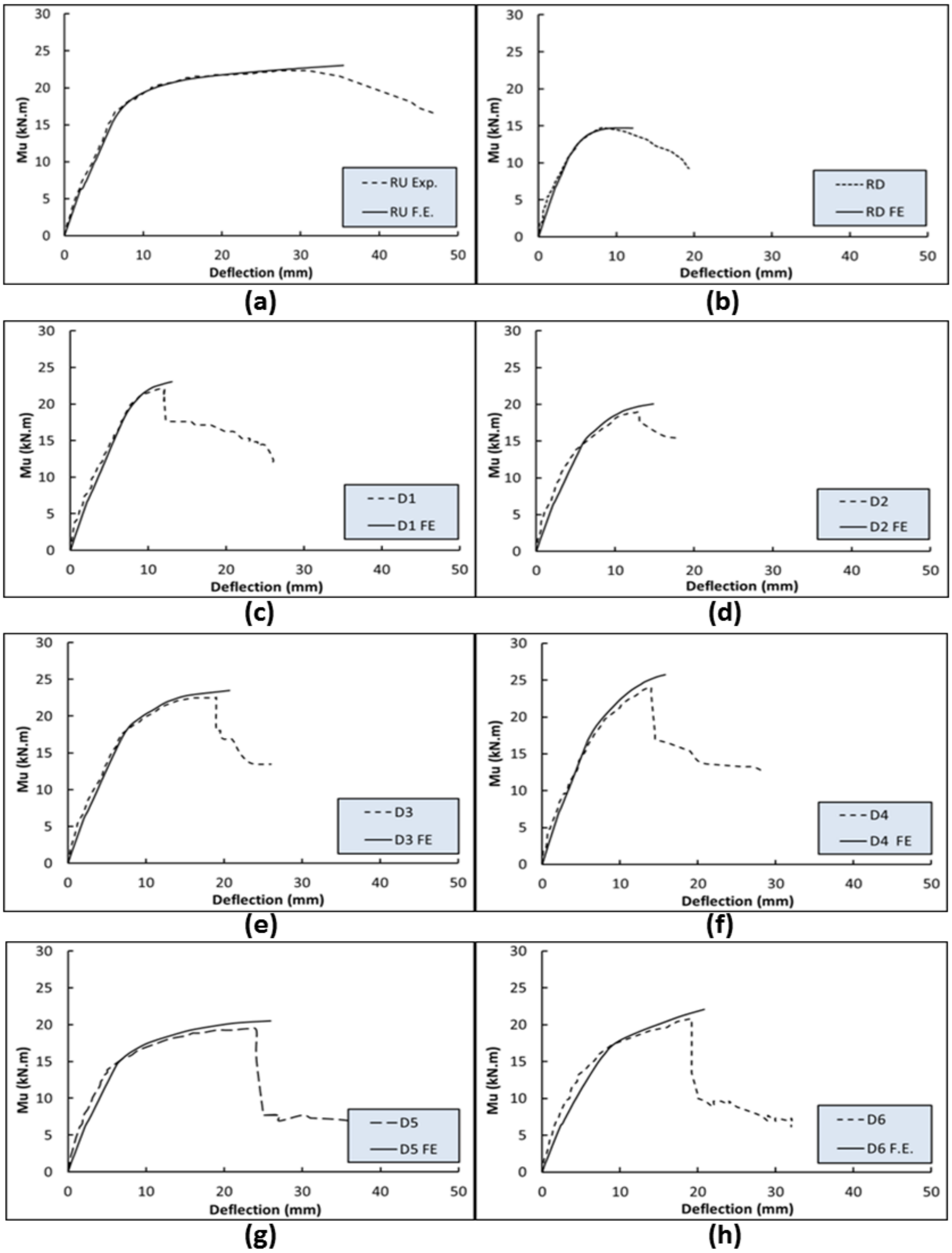

Fig. 11 Finite element and experimental moment-deflection relations: (a)Beam RU; (b) Beam RD; (c) Beam D1; (d) Beam D2; (e) Beam D3; (f) Beam D4; (g) Beam D5; (h) Beam D6

material. The material properties in the fiber direction were considered as provided by the manufacturer and as listed earlier in Table 3. In any other direction than the fiber direction, the properties were considered the same as the adhesive properties. The shear moduli were calculated according to Eq. (4), where E, G, υ are the elastic modulus, shear modulus and poisson's ratio respectively.

$$E_c = f/\varepsilon \tag{1}$$

$$f = E_c.\varepsilon \,/\, [1 + (\varepsilon/\varepsilon_0)^2] \tag{2}$$

$$\varepsilon_0 = 2f_c^{'}/E_c \tag{3}$$

$$G_{xy} = E/[2(1 + \upsilon_{xy})] \tag{4}$$

5. Finite Element model validation

The finite element simulation has been carried out using the above model and it was standardized against the experimental data. The validation based on the ultimate moment and the corresponding deflection value, moment-deflection curves and failure modes of all studied CFST beams.

5.1 Moment-deflection relationship

Fig. 11 shows the comparison between moment-deflection relationships measured experimentally and numerically for the reference CFST beams and repaired beams. It is clear that the finite element results match very well the experimental data from the onset of loading until failure. In experimental testes, the load drops suddenly when the FRP batches rupture or debonding occurs between these batches and the steel tube. This bahaviour is common in steel beams repaired with FRP material; Seica and Packer (2007), Deng and Lee (2007), Kabir *et al*. (2016). However, the finite element analysis stops when any of the failure criteria in any part of the model takes place and it cannot depict this phenomenon. The same behaviour was reported by many other researchers studied the FRP-steel bond issue using different finite element packages as Teng *et al*. (2015) and Kabir *et al*. (2016).

5.2 Ultimate moment and corresponding deflection

The values of ultimate moments and the corresponding deflections of the tested CFST un-damaged, damaged reference beams and all repaired beams using CFRP and GFRP batches are illustrated in Table 5. The maximum ratio between the ultimate moment capacity of the experimentally studied beams and their finite element simulation was about 6.9%. Reasonable values were obtained for the mid-span deflections as well. These comparisons provided small values of COV of all studied specimens; about 0.02 for ultimate moment and 0.04 for the corresponding deflections. This demonstrates the ability of the proposed finite element model for simulating the CFST beam repaired with FRP.

5.3 Failure modes

Local buckling at the top flange of the steel tube, FRP rupture, debonding between the FRP batch and the steel tube and crack propagation in the steel tube were the most recognized failure modes in the tested specimens. Local buckling at the top flange of the steel tube was the common failure mode between all the tested specimens. This mode of failure was clear in all of the modeled beams in the finite element analyses. A typical shape of this buckling is shown in Fig. 12(a). The figure shows also the crack propagation in the steel tube. Debonding between FRP sheets and the steel tube was noticed in the finite element models through the contact status. The edge of the FRP batch was separated; as in beam D1 in Fig. 12(b) as an example; and sliding was clear in the following elements. Rupture in the FRP sheet was clear as well and it was noticed through the high stresses concentrated at the rupture position. Fig. 12(c) shows rupture in the CFRP sheet at the middle of the beam in model of D2 as an example. Although the finite element model indicated that the failure was due to rupture in the CFRP sheet, however the gradual failure which happened in the experimental test of D2 could not be recognized in the analysis. This is because the analysis always stops when any of the failure criteria occurs.

Table 5 Comparison between experimental and FE results

Beam	Experimental		Finite Element		$\frac{M_{u.FE}}{M_{u.Exp}}$	$\frac{\Delta_{u.FE}}{\Delta_{u.Exp}}$
	$M_{u.\mathrm{Exp}}$ (kN.m)	$\Delta_{\mathrm{u.Exp}}$ (mm)	$M_{u.\mathrm{FE}}$ (kN.m)	$\Delta_{\mathrm{u.FE}}$ (mm)		
RU	22.30	30.50	23.04	35.44	1.033	1.162
RD	14.63	9.80	14.70	11.10	1.005	1.133
D1	22.12	12.10	23.05	13.03	1.042	1.077
D2	18.86	13.20	20.06	14.05	1.064	1.064
D3	22.56	19.50	23.48	20.29	1.041	1.041
D4	24.10	14.20	25.76	15.11	1.069	1.064
D5	19.44	23.30	20.50	25.13	1.055	1.079
D6	20.80	19.60	22.09	20.72	1.062	1.057
		COV			0.02	0.04

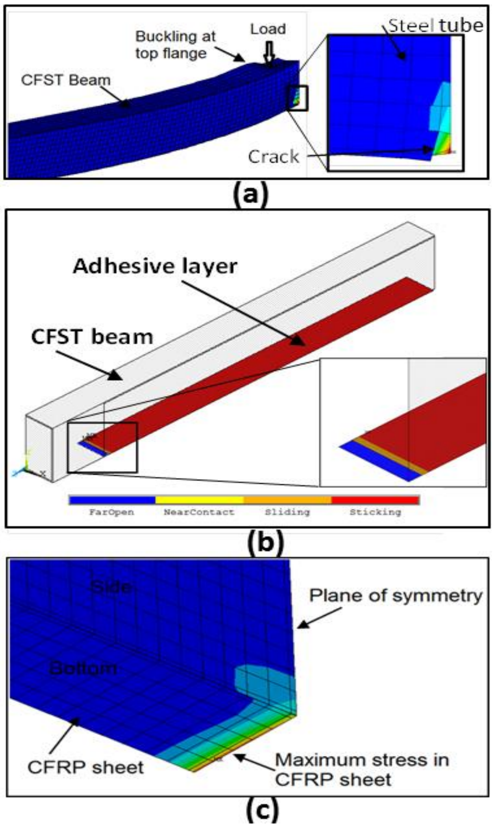

Fig. 12 Finite element failure shapes

6. Retrofitting effect on CFST beams

With the aid of the validated finite element model, the effect of some parameters on the behavior of repaired square CFST beams is investigated herein.

6.1 Effect of FRP repairing on concrete core

The cracking and crushing capabilities available in the

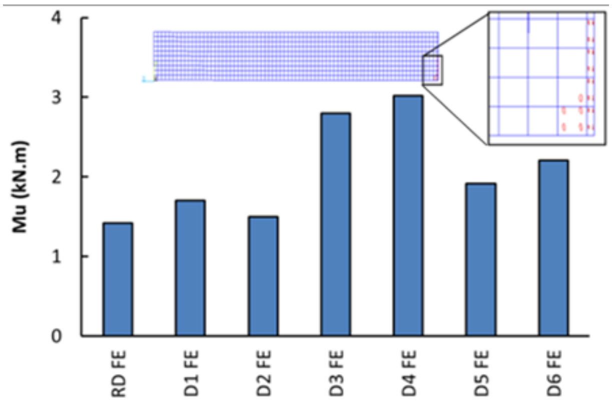

Fig. 13 Effect of FRP retrofitting on concrete cracking

solid element which was used for modeling the concrete core enabled monitoring initiation and progression of cracked and crushed elements. Fig. 13 illustrates the values of the moments at which the concrete core began to crack at the middle of the beam. It is clear from the chart that increasing the number of layers around the crack position delayed the crack initiation. The maximum effect was recognized in beams (D3 F.E.) and (D4 F.E.) which were repaired with CFRP sheets. Although the same retrofitting schemes were used in beams D5 FE and D6 FE (but with GFRP instead of CFRP), the moment value at which the crack in concrete started was noticeably lower. This may be due to the lower elastic modulus of the GFRP material which permitted higher deflection in the beam.

6.2 Effect of CFRP tensile modulus

FRP tensile modulus is one of the effective parameters on the repaired members. Three different values of CFRP elastic modulus (150 Gpa, 234 Gpa and 552 Gpa) were used to investigate the change in the repaired CFST beam behavior. All beams were repaired by two layers of CFRP with thickness of 0.128 mm each and the sheet covered the full effective beam length. Fig. 14(a) shows the increase in the repaired beam ultimate moment by about 11.7% and 20.3%, when using CFRP with elastic moduli of 234 Gpa and 552 Gpa than the beam repaired by CFRP sheet with elastic modulus of 150 Gpa. However, a reversible effect was noticed on the beam ductility. The corresponding decreases in these beams deflection were 6% and 28% respectively.

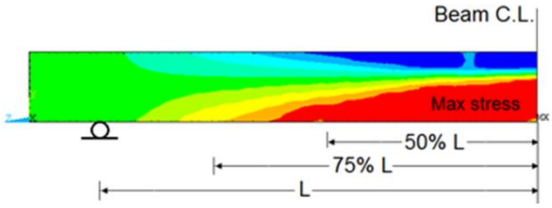

Fig. 15 Stress distribution in CFST beam

6.3 Effect of number of CFRP layers

Fig. 14(b) demonstrates the influence of using several layers of CFRP sheets on the repaired CFST beam behavior. The CFRP sheet covered the full effective length of the beam with the same CFRP thickness. The figure shows an enhancement in the ultimate moment capacity of the repaired CFST beam with one layer of CFRP sheet by 26.4% in comparison to the notched beam without repairing. The rate of this increase diminishes with the increase of the number of layers since using 2, 3 and 4 layers increased the ultimate capacity of the notched beam by 54%, 67% and 77%, respectively. On the other hand, a dramatic decrease in the beam deflection was noticed as the number of CFRP layers increased. As described above, the different layers of the CFRP sheet were modeled by using the multilayer option in the used ANSYS element, as there was no separation between the different layers in the experimental tests. Using more layers for the element, which increases the total thickness of the element, increased the peeling stress at the end of the bonded CFRP sheet. This was avoided when using higher tensile modulus of CFRP sheet without increasing the number of layers.

6.4 Effect of CFRP length

Three U-shape retrofitting lengths were examined; covering 100%, 75% and 50% of the beam clear span. All of the repairing lengths composed of two layers of CFRP sheets. Fig. 14(c) compares the ultimate moment and the mid-span deflection of the CFST beams for the different lengths. As the length of the CFRP sheet increased, the ultimate moment increased. It was found that the relative moment increment was minimal when the CFRP length was 75% L and more. This is may be due to that in these beams the CFRP covered the highly stressed region of the beam, as illustrated in Fig. 15. A small decrease in the beam

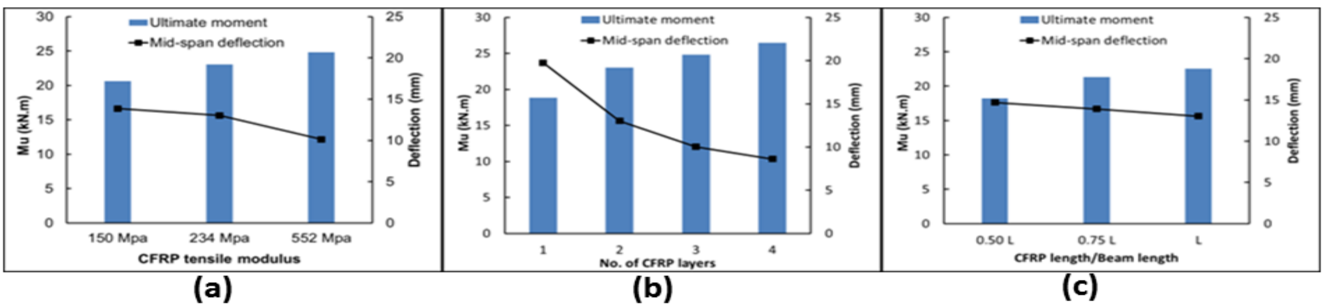

Fig. 14 Effect of (a) CFRP tensile modulus (b) number of CFRP layers (c) CFRP length, on Repaired CFST bea

deflection was noticed when increasing the total length of the CFRP sheet, as shown in Fig. 14(c).

7. Conclusions

In this paper, the structural behavior of FRP repaired square CFST beams have been investigated experimentally and numerically. The results of eight CFST tested under four point bending were discussed. A 3-D FE model was developed for un-repaired and repaired tested beams. After proving the model accuracy, a range of parameters were conducted. The following are the main conclusions:

- Using CFRP sheets to repair notched CFST square beams increased its ductility index by about 20% to 32.7% according to the retrofitting scheme. However, none of these schemes managed to restore the ductility of the unrepaired un-notched reference beam.
- GFRP sheets provided an enhancement of about 5.3% in the ductility of the repaired square CFST beams than that provided by using CFRP sheets with the same number of layers and repairing schemes, while, the ultimate beam capacity was reduced by about 21%.
- Longitudinal FRP rupture in high bending stress region could be avoided by repairing the CFST beam by one with fibers parallel to the beam and another with fibers transverse to the beam. However its effect on beam capacity was about 56% of the capacity gained when using two FRP layers parallel to the beam.
- Providing different cut-off points for the different layers of FRP sheets prevented failure at termination points.
- The proposed FE model accurately predicted the moment-deflection relations, ultimate moment and failure modes of reference beams and repaired beams with different repairing schemes and FRP types. The COV for moment capacity was about 0.02 and for deflection was about 0.04.
- Wrapping the notched CFST beams with four layers of U-shape CFRP sheets increased the moment-carrying capacity up to 77%. U-wrapping of notched CFST beam with 0.75 of its length provided a comparable behavior as wrapping the full length of the beam, since these lengths covered the high stressed regions of the beam.
- Increasing number of layers around the crack positions increased the cracked beam capacity and delayed crack initiation in the concrete core. A reduced effect was noticed when using the same area of GFRP sheets, due to its low elastic modulus which permits higher deflection.

Using higher tensile modulus of FRP sheet is better than increasing the number of layers of FRP sheet since increasing the total thickness of the FRP sheet increases the peeling stress at FRP sheet edge.

Acknowledgments

The author would like to thank, Zagazig University for providing support to perform the reported work. The author gratefully thanks the members of the structural laboratory for their great assistance in conducting the experimental work in faculty of engineering, ZU.

References

Al Zand, A.W., Badaruzzaman, W.H.W., Mutalib, A.A. and Qahtan, A.H. (2015), “Finite element analysis of square CFST beam strengthened by CFRP composite material”, *Thin-Wall. Struct*., **96**, 348-358.

Al Zand, A.W., Badaruzzaman, W.H.W., Mutalib, A.A. and Hilo, S.J. (2016), “The enhanced performance of CFST beams using different strengthening schemes involving unidirectional CFRP sheets: An experimental study”, *Eng Struct*, **128**, 184-198.

Al Zand, A.W., Badaruzzaman, W.H.W., Mutalib, A.A. and Hilo, S.J. (2017), “Rehabilitation and strengthening of high-strength rectangular CFST beams using a partial wrapping scheme of CFRP sheets: Experimental and numerical study”, *Thin-Wall. Struct*., **114**, 80-91.

ANSYS (2013), Element Manual; Release 15, Swanson Analysis Systems, Canonsburg, PA, USA.

ASTM-E8/E8M (2009), Standard test methods for tension testing of metallic materials; West Conshohocken, PA, USA.

Chen, T., Qi, M., Gu, X.L. and Yu, Q.Q. (2015), “Flexural strength of carbon fiber reinforced polymer repaired cracked rectangular hollow section steel beams”, *Int. J. Polym. Sci*., **9**.

Colombi, P. and Fava, G. (2015), “Experimental study on the fatigue behaviour of cracked steel beams repaired with CFRP plates”, *Eng. Fract. Mech*., **145**, 128-142.

Deng, J. and Lee, M.M.K. (2007), “Behaviour under static loading of metallic beams reinforced with a bonded CFRP plate”, *Compos Struct*., **78**, 232-242.

Elchalakani, M. (2014a), “CFRP strengthening and rehabilitation of degraded steel welded RHS beams under combined bending and bearing”, *Thin-Wall. Struct*., **77**, 86-108.

Elchalakani, M. (2014b), “Plastic collapse analysis of CFRP strengthened and rehabilitated degraded steel welded RHS beams subjected to combined bending and bearing”, *Thin-Wall. Struct*., **82**, 278-295.

Fawzia, S., Al-Mahaidi, R. and Rizkalla, S. (2007), “Strengthening of circular hollow steel tubular sections using high modulus CFRP sheets”, *Construct. Build. Mater*., **21**, 839-845.

Gere, J.M. (1997), “Timoshenko SP Mechanics of Materials”, PWS, Boston, MA, USA.

Kabir, M.H., Fawzia, S., Chan, A., Gamage, B. and Bai, J.B. (2016), “Experimental and numerical investigation of the behaviour of CFRP strengthened CHS beams subjected to bending”, *Eng. Struct*., **113**, 160-173.

Kim, Y.J. and Harries, K.A. (2011), “Fatigue behavior of damaged steel beams repaired with CFRP strips”, *Eng. Struct*., **33**, 1491-1502.

Mahdi, I., Setvati, R. and Mustaffa, Z. (2018), “Rehabilitation of notched circular hollow sectional steel beam using CFRP patch”, *Steel Compos. Struct., Int. J*., **26**(2), 151-161.

Photiou, N.K., Hollaway, L.C. and Chryssanthopoulos, M.K. (2006), “Strengthening of an artificially degraded steel beam utilizing a carbon/glass composite system”, *Construct. Build. Mater*., **20**,11-21.

Sallam, H. (2010), “Discussion of “Flexural strengthening of steel bridges with high modulus CFRP strips”, (by David Schnerch and Sami Rizkalla), *J. Bridge Eng*., **15**(1), 117-117.

DOI: 10.1061/(ASCE)1084-0702(2008)13:2(192)
Sallam, H., Badawy, A., Saba, A. and Mikhail, F. (2010), "Flexural behavior of strengthened steel_concrete composite beams by various plating methods", *J. Constr. Steel Res.*, **66**, 1081-1087.
Seica, M.V. and Packer, J.A. (2007), "FRP materials for the rehabilitation of tubular steel structures, for underwater applications", *Compos. Struct.*, **80**(3), 440-450.
Sen, R. and Liby, L. (1994), "Repair of steel composite bridge sections using CFRP laminates", U.S. Department of Transportation Contract B-7932, University of South Florida, Tampa, FL, USA.
Sundarraja, M.C. and Prabhu, G.G. (2013), "Flexural behaviour of CFST members strengthened using CFRP composites", *Steel Compos. Struct., Int. J.*, **15**(6), 623-643.
Tavakkolizadeh, M. and Saadatmanesh, H. (2003), "Repair of damaged steel-concrete composite girders using carbon fiber-reinforced polymer sheets", *J. Compos. Constr.*, **7**, 311-322.
Teng, J.G. and Hu, Y.M. (2007), "Behaviour of FRP-jacketed circular steel tubes and cylindrical shells under axial compression", *Constr. Build. Mater.*, **21**(4), 827-838.
Teng, J.G., Fernando, D. and Yu, T. (2015), "Finite element modelling of debonding failures in steel beams flexurally strengthened with CFRP laminates", *Eng. Struct.*, **86**, 213-224.
Yang, Y.X., Yue, Q.R. and Peng, F.M. (2005), "Experimental research on bond behavior of CFRP to steel", *Proceedings of the International Symposium on Bond Behaviour of FRP in Structures*, pp. 419-422.
Yousefi, O., Narmashiri, K. and Ghaemdoust, M.R. (2017), "Structural behaviors of notched steel beams strengthened using CFRP strips", *Steel Compos. Struct., Int. J.*, **25**(1), 35-43.
Zhao, X.L. and Zhang, L. (2007), "State-of-the-art review on FRP strengthened steel structures", *Eng. Struct.*, **29**, 1808-1823.
Zhong, T. and Han, L.H. (2007), "Behaviour of fire-exposed concrete-filled steel tubular beam columns repaired with CFRP wraps", *Thin-Wall. Struct.*, **45**, 63-76.
Zhong, T., Han, L.H. and Wang, L.L. (2007), "Compressive and flexural behaviour of CFRP-repaired concrete-filled steel tubes after exposure to fire", *J. Constr. Steel Res.*, **63**, 1116-1126.

CC